Astrocyte-derived lipoxins A_4 and B_4 promote neuroprotection from acute and chronic injury

Izhar Livne-Bar,[1,2] Jessica Wei,[3] Hsin-Hua Liu,[3] Samih Alqawlaq,[1,2,4] Gah-Jone Won,[1,2] Alessandra Tuccitto,[1,2,4] Karsten Gronert,[3] John G. Flanagan,[3] and Jeremy M. Sivak[1,2,4]

[1]Department of Vision Sciences, Krembil Research Institute, University Health Network, Toronto, Ontario, Canada. [2]Department of Ophthalmology and Vision Science, University of Toronto, Toronto, Ontario, Canada. [3]Vision Science Program, School of Optometry, University of California at Berkeley, Berkeley, California, USA. [4]Department of Laboratory Medicine and Pathobiology, University of Toronto, Toronto, Ontario, Canada.

Astrocytes perform critical non–cell autonomous roles following CNS injury that involve either neurotoxic or neuroprotective effects. Yet the nature of potential prosurvival cues has remained unclear. In the current study, we utilized the close interaction between astrocytes and retinal ganglion cells (RGCs) in the eye to characterize a secreted neuroprotective signal present in retinal astrocyte conditioned medium (ACM). Rather than a conventional peptide neurotrophic factor, we identified a prominent lipid component of the neuroprotective signal through metabolomics screening. The lipoxins LXA_4 and LXB_4 are small lipid mediators that act locally to dampen inflammation, but they have not been linked directly to neuronal actions. Here, we determined that LXA_4 and LXB_4 are synthesized in the inner retina, but their levels are reduced following injury. Injection of either lipoxin was sufficient for neuroprotection following acute injury, while inhibition of key lipoxin pathway components exacerbated injury-induced damage. Although LXA_4 signaling has been extensively investigated, LXB_4, the less studied lipoxin, emerged to be more potent in protection. Moreover, LXB_4 neuroprotection was different from that of established LXA_4 signaling, and therapeutic LXB_4 treatment was efficacious in a chronic model of the common neurodegenerative disease glaucoma. Together, these results identify a potential paracrine mechanism that coordinates neuronal homeostasis and inflammation in the CNS.

Introduction

Astrocytes and related macroglia perform critical non–cell autonomous roles mediating parainflammatory signals following CNS injury (1, 2). Previous work on this activity has focused on induced neurotoxic signals, though neuroprotective roles have also been described from distinct astrocyte populations (3–6). However, the nature of these protective signals has remained unclear. The inner retina provides an accessible neuronal injury model, where progressive damage is a hallmark of the common and incurable neurodegenerative disease glaucoma (7, 8). In this neurovascular tissue, vulnerable retinal ganglion cells (RGCs) interact intimately with neighboring astrocytes and related Müller glia (9, 10). Non–cell autonomous signaling has been strongly implicated in stress-induced parainflammation and RGC damage, with emphasis on neurotoxic TNF-α secreted by reactive astrocytes (11–13). We recently reported that inhibition of this mechanism promotes RGC survival following acute injury (14). Yet a model of induced neurotoxic glial reactivity was not sufficient to trigger RGC death, suggesting that a concomitant loss of protective activity is also involved (14). Here we have utilized an established model of primary retinal astrocytes (RAs) to characterize a secreted neuroprotective signal present in astrocyte conditioned medium (ACM). Through biochemical characterization and metabolomic screening, we have surprisingly identified that a prominent component of this protective signal is mediated via small lipid mediators, rather than a conventional peptide neurotrophic factor. These mediators, the lipoxins LXA_4 and LXB_4, are highly enriched in protective ACM.

Lipoxins are autacoids, specialized proresolving lipid mediators (SPMs) that act locally in a paracrine or autocrine manner and are rapidly metabolized. They belong to a super family of small polyunsaturated fatty acid–derived (PUFA-derived) metabolites, which direct potent cellular responses to dampen inflammation and restore homeostasis (15, 16). SPMs derived from docosahexaenoic acid (DHA), including resolvins, maresins, and protectins, have recently been investigated for roles in neuroinflammation (17, 18). In contrast, a direct role for lipoxins in neuroprotection has not been explored. Lipoxins were the first identified SPMs and are arachidonic acid–derived (AA-derived) eicosanoids formed by sequential oxygenation via the conserved lipoxygenase enzymes 5-LOX and 15-LOX (19, 20). The 2 endogenous lipoxins LXA_4 and LXB_4 display a range of antiinflammatory and proresolving activities. LXA_4 binds with high affinity to the GPCR formyl peptide receptor 2 (ALX/FPR2) to mediate leukocyte recruitment, angiogenesis, and inhibition of NF-κB–induced IL-6 and TNF-α (19, 21). Dysregulated LXA_4 and lipoxygenases have been associated with neuroinflammatory roles (22–24), but have not been reported to

Authorship note: I. Livne-Bar, J. Wei, and H.H. Liu contributed equally to this work. K. Gronert, J.G. Flanagan, and J.M. Sivak are co–senior authors.
Conflict of interest: The authors have declared that no conflict of interest exists.
Submitted: June 19, 2017; **Accepted:** September 26, 2017.
Reference information: *J Clin Invest*. 2017;127(12):4403–4414.
https://doi.org/10.1172/JCI77398.

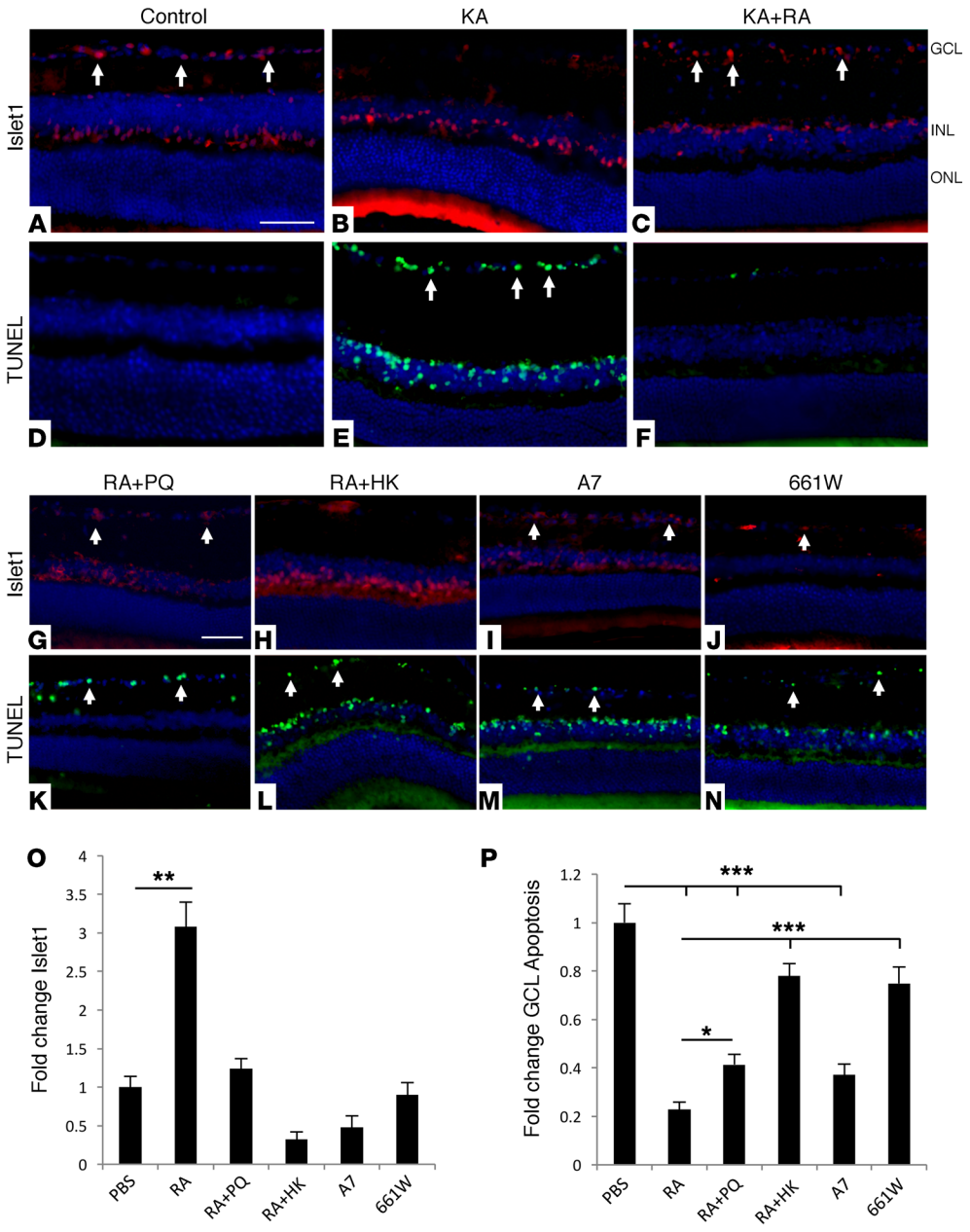

Figure 1. Transplanted RAs protect inner retinal neurons in vivo. (**A**–**C**) Transplantation of RAs increased survival of GCL and INL neurons following KA-induced injury, compared with PBS-injected controls (Islet1: red, arrows). INL, inner nuclear layer; ONL, outer nuclear layer. (**D**–**F**) Adjacent sections were TUNEL stained (green, arrows), and show a complementary pattern, with reduced apoptosis GCL and INL in eyes with transplanted RAs. (**G**–**H**) Rescue of Islet1-positive neurons was reduced or absent when RAs were prestressed by treatment with 300 μM PQ (RA+PQ) or heat killed (RA+HK). (**I** and **J**) Transplants of A7 or 661W cells were also not protective. (**K**–**N**) Corresponding TUNEL staining showed higher GCL or INL apoptosis in the controls compared with RA transplants. (**O**) Quantification of Islet1 results for each group, showing significant protection of GCL neurons by RAs that is absent in each of the controls (n = 10). (**P**) Quantification of TUNEL results for each group, showing a significant reduction of apoptosis by RAs that is lower or absent in the controls (n = 10). Scale bars: 50 μm. $^{*}P < 0.05$; $^{**}P < 0.01$; $^{***}P < 0.005$ compared with PBS. Bars represent SEM. Statistical analyses were performed by 1-way ANOVA with TUKEY post-hoc test.

have direct neuronal actions. The activities of LXB_4 are distinct from those of LXA_4 and include potent effects on macrophages and nonphlogistic monocyte activation (25, 26). Yet LXB_4 has been far less studied than LXA_4, in part because reliable commercial sources have only recently become available. There is consequently little knowledge about LXB_4 functions in the CNS or roles in neurodegeneration.

Here, we report that LXA_4 and LXB_4 are highly enriched in ACM and demonstrate their direct neuroprotective activity. We characterize their biosynthesis and roles in inner retinal injury and discover unexpectedly higher activity for LXB_4, independent of LXA_4 signaling. Finally, we demonstrate that therapeutic LXB_4 administration is functionally and pathologically efficacious in a chronic glaucoma model, suggesting that strategies to rescue this astrocytic signal may be relevant to treatment of neurodegeneration.

Results

Transplanted RAs exhibit neuroprotective activity that is compromised by stress. We have previously extensively characterized astrocytes cultured from the adult retina and optic nerve (ON) head (27–29). These cells display typical astrocyte morphology and markers, and respond robustly to stress (27) (Supplemental Figure 1; supplemental material available online with this article; https://doi.org/10.1172/JCI77398DS1). We studied the effects of RAs on inner retinal neurons by transplanting them into recipient C57BL/6 eyes. After 16 days, transplants remained viable and showed minimal inflammatory infiltrates, cell death, or endogenous glial activation (Supplemental Figure 2). Transplant eyes were challenged after 16 days with injection of kainic acid (KA). Similar excitotoxic models of inner retinal metabolic injury have been previously demonstrated to be dependent on glial

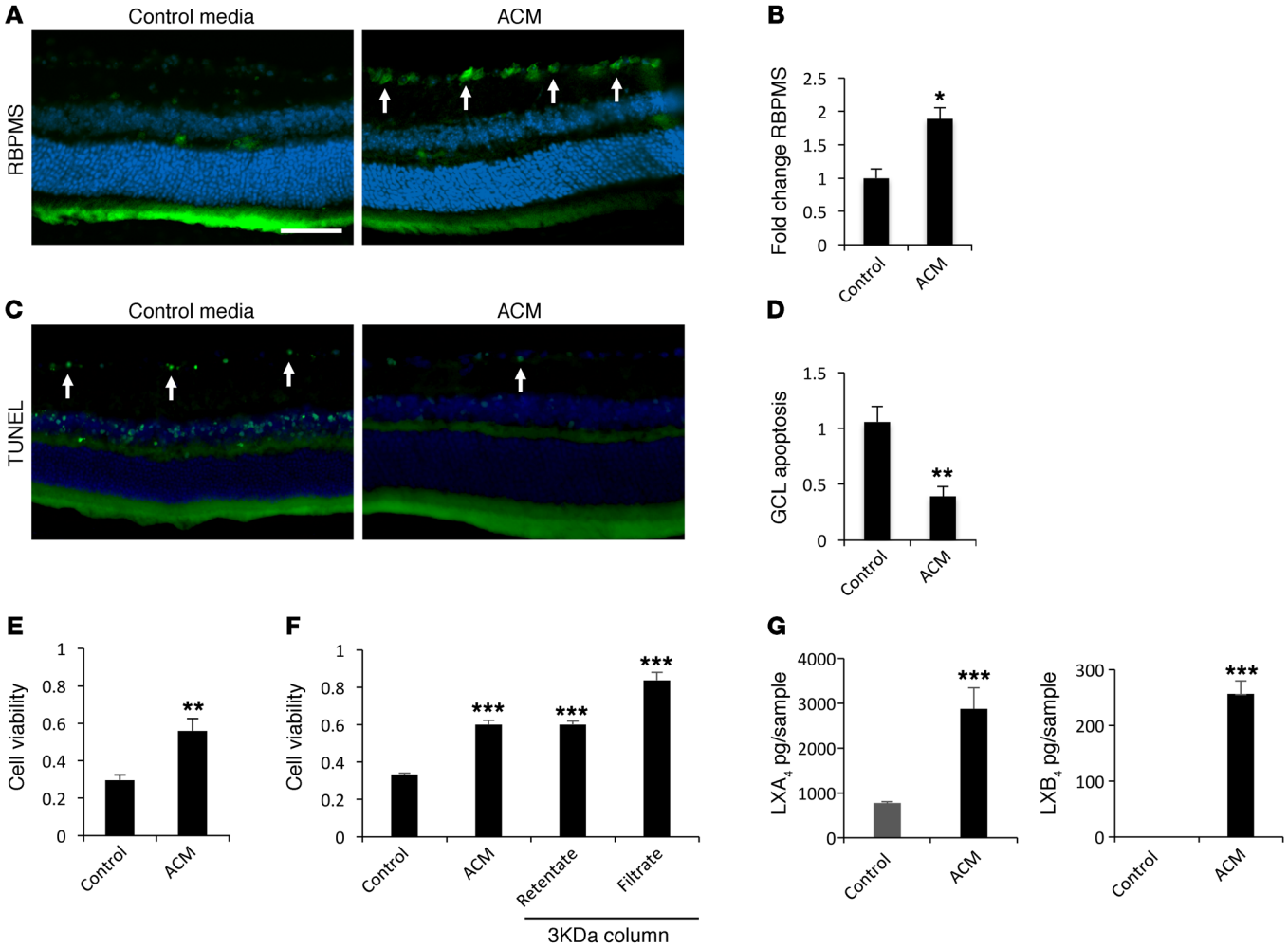

Figure 2. Astrocyte neuroprotection is mediated by a small secreted activity that is enriched in lipoxins. ACM or cell-free control media was injected intravitreally 1 day prior to KA challenge. (**A**) ACM treatment reduced KA-induced RGC loss compared with cell-free control media (RBPMS: green, arrows). (**B**) Quantification of RBPMS results showing significant RGC survival with ACM injection ($n = 5$). (**C**) Complimentary results showing ACM-mediated reduction in TUNEL-labeled cells (green, arrows) compared with control media. (**D**) Quantification of TUNEL results showing significant decrease in GCL apoptosis from ACM media ($n = 5$). (**E**) ACM protection was reproduced in vitro with HT22 neuronal cells challenged with 5 mM glutamate ($n = 3$). (**F**) Substantial protective activity in ACM is contained in a 3-kDa filtrate ($n = 3$). (**G**) High concentrations of LXA_4 and LXB_4 were detected in ACM compared with control media by LC-MS/MS ($n = 3$). Scale bar: 50 μm. $^*P < 0.05$; $^{**}P < 0.01$; $^{***}P < 0.005$. Bars represent SEM. Statistical analyses were performed by 1-way ANOVA with TUKEY post-hoc test.

function (12, 14, 30). Remarkably, we found that RA transplants strongly protected neurons in the ganglion cell layer (GCL) (Figure 1, A–C). In complementary studies, TUNEL staining found a marked reduction of GCL apoptosis in transplanted eyes compared with PBS controls (Figure 1, D–F). As further controls, RAs were first exposed to oxidative stress with the redox agent paraquat (PQ) (Figure 1G) (27) or heat-killed to control for generalized inflammatory effects (Figure 1H). Neither treatment rescued GCL neurons, nor did injection of immortalized astrocytic A7 cells or 661W neuronal cells (Figure 1, I and J). Complementary results were likewise obtained through TUNEL staining (Figure 1, K–N). Following quantification, RA-transplant eyes showed a significant ($P < 0.01$) 3-fold rescue of GCL neurons compared with PBS control, while the additional controls offered reduced or no protection (Figure 1, O and P). These experiments indicate that RAs actively provide neuroprotective support.

RA neuroprotection is mediated through small secreted factors enriched in LXA_4 and LXB_4. The protective activity produced by transplanted RAs could be driven by endogenous detoxifying mechanisms or secreted signals. To distinguish these possibilities, we collected ACM and tested whether it was sufficient to provide protection. Either ACM or cell-free control media incubated under identical conditions was injected intravitreally into C57BL/6 mice 24 hours prior to KA challenge. RGC survival was specifically assessed by probing for the marker RBPMS, along with complementary TUNEL staining and quantification. Significant rescue of RGCs was observed in eyes injected with ACM compared with control media ($P < 0.05$) (Figure 2, A and B), while TUNEL staining showed that ACM injection strongly reduced GCL death ($P < 0.01$) (Figure 2, C and D). To facilitate further study, we established an in vitro assay in which ACM was applied to the neuronal cell line HT22. Consistent with the in vivo results, ACM treatment

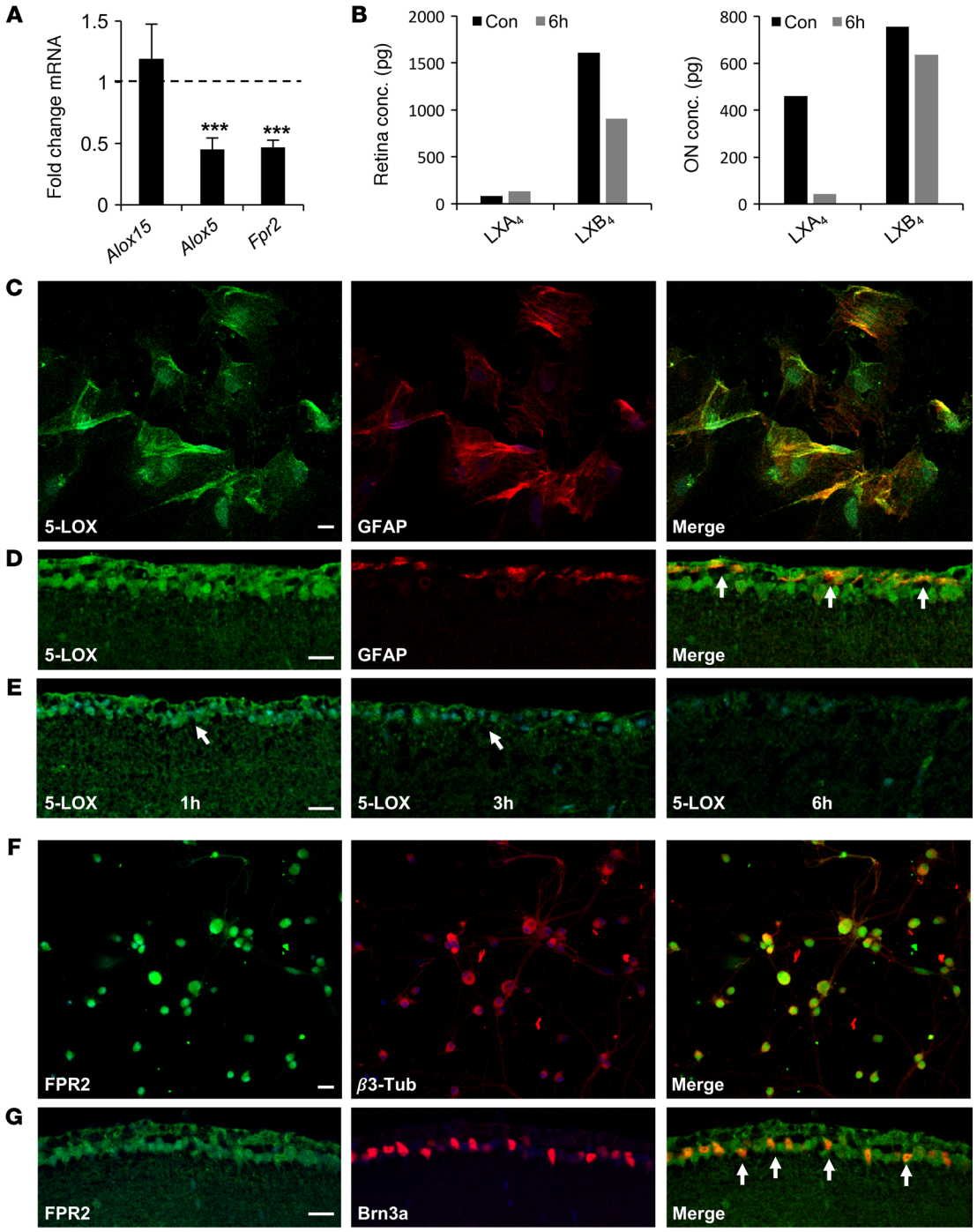

Figure 3. Lipoxins are regulated in the inner retina in response to acute injury. (**A**) qPCR of mouse retinal cDNAs shows significantly reduced expression of *Alox5* and *Fpr2*, but not *Alox15*, 2 hours after KA insult compared with PBS controls (n = 3). (**B**) LXB_4 concentrations in total mouse retina are reduced at 6 hours following injury, while LXA_4 concentrations are reduced in the ON compared with PBS-injected controls (n = 10 retinas/aggregate group). (**C**) Confocal microscopy shows 5-LOX immunostaining in primary RAs. (**D**) Confocal imaging of 5-LOX immunostaining (green) shows accumulation in the GCL and NFL, with partial colocalization (yellow, arrows) in astrocytes (GFAP: red). (**E**) Signal for 5-LOX in the inner retina is reduced at 3 and 6 hours after injury (arrows). (**F**) FPR2 immunostaining (green) is prominent in cultured primary RGCs stained with β3-tubulin (red). (**G**) ALX/FPR2 immunostaining (green) is specific to the GCL and colocalizes (yellow, arrows) with RGCs (Brn3a: red). Scale bars: 20 μm (**C** and **F**); 10 μm (**D** and **G**). ***$P < 0.005$. Bars represent SEM. Statistical analyses were performed by 1-way ANOVA with TUKEY post-hoc test.

produced significant HT22 cell protection from glutamate challenge ($P < 0.01$) (Figure 2E). These data established a platform for future studies of the ACM activity. Surprisingly, in preliminary fractionation experiments, we discovered that a substantial portion of protective activity was contained in filtrate smaller than 3 kDa, ruling out most common neurotrophic factors (Figure 2F).

In order to identify small molecules in the ACM that might account for the protective activity, we performed metabolomic

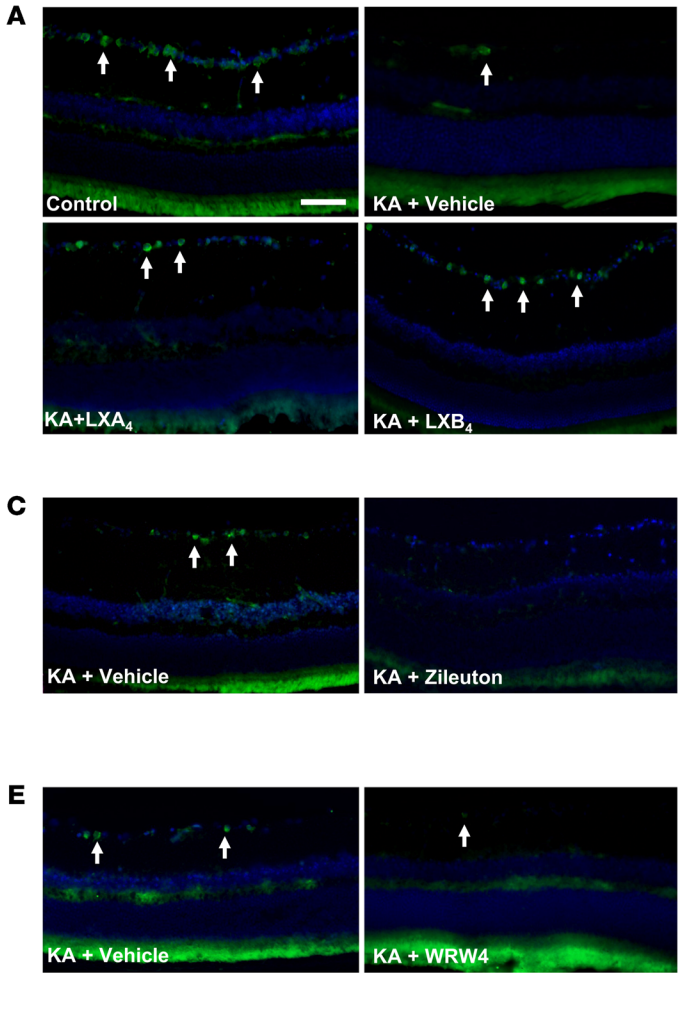

Figure 4. LXA_4 and LXB_4 promote RGC survival following acute injury. (**A**) Intravitreal injection of 10 μM LXA_4 or LXB_4 prior to KA-induced insult resulted in increased RGC survival compared with control (PBS) (RBPMS: green, arrows). (**B**) Corresponding quantification shows significant increases in RGC survival with LXA_4 or LXB_4 treatment compared with vehicle control. Values are presented as fold change from noninjured controls (n = 8). (**C** and **D**) In contrast, intravitreal treatment with 10 μM of the 5-LOX inhibitor zileuton significantly compromised RGC survival following acute stress compared with vehicle (n = 5). (**E** and **F**) Similarly, 15 μM of the ALX/FPR2 inhibitor WRW4 significantly reduced RGC survival following acute stress compared with vehicle (n = 5). Scale bar: 50 μm. *$P < 0.05$. Bars represent SEM. Statistical analyses were performed by 1-way ANOVA with TUKEY post-hoc test.

screening, including an assessment of SPMs, using liquid chromatography–tandem mass spectrometry (LC-MS/MS). Lipid mediators were quantified to generate a lipidomic profile of SPMs, including eicosanoids and PUFAs. Pathway markers for DHA-derived resolvins and protectins were detected (DHA, 17-HDHA), but not their direct formation. In contrast, lipidomic analyses revealed significant enrichment of the lipoxins LXA_4 and LXB_4 in ACM compared with control media (Figure 2G). DHA is highly enriched in the retina, but can be regulated by diet. Hence, we cannot exclude the possibility that the absence of resolvins and protectins in ACM reflects dietary DHA intake.

LXA_4 and LXB_4 biosynthesis and signaling are regulated in the inner retina. To corroborate the presence of lipoxin signaling in the mouse retina, we used quantitative reverse-transcription PCR (qPCR) to assess expression of *Alox5* and *Alox15* as well as the LXA_4 receptor *Fpr2* (mouse orthologs of *5-LOX*, *15-LOX-1*, and *FPR2*, respectively). All 3 transcripts were detected, and expression of *Alox5* and *Fpr2*, but not *Alox15*, was significantly reduced following retinal insult ($P < 0.005$) (Figure 3A). Due to their short half-life and rapid metabolic inactivation, endogenous lipoxins can be challenging to detect in small tissue samples. However, by pooling 10 retinas, we were able to quantify aggregate LXA_4 and LXB_4 concentrations in control eyes and at 6 hours following injury. In retina samples, baseline LXA_4 levels were low and did not change following insult. However, levels of LXB_4 were reduced by nearly 50% (Figure 3B). In addition to total retina concentrations, we also assessed lipoxin levels in pooled ONs, which are enriched in astrocytes. In these samples, LXA_4 levels were dramatically reduced by 6 hours after injury, with a small reduction of LXB_4 (Figure 3B).

As 5-LOX is the rate-limiting enzyme for LXA_4 and LXB_4 formation, we confirmed its presence in cultured RAs (Figure 3C). Localized 5-LOX immunoreactivity was also present in the inner retina in astrocytes and RGCs (Figure 3D). Consistent with our qPCR results, retinal insult reduced the 5-LOX signal by 3 and 6 hours (Figure 3E). In comparison, immunostaining demonstrated ALX/FPR2 protein in RGCs in vitro and in vivo (Figure 3, F and G). These data suggest that the lipoxin circuit, comprising biosynthetic enzymes and the LXA_4 receptor, is present in the inner retina and that its functional activity is compromised in response to injury.

LXA_4 and LXB_4 promote RGC survival following acute insult. We next asked whether treatment with LXA_4 or LXB_4 is sufficient to promote RGC protection in vivo. To test this point, 10 μM LXA_4 or LXB_4 was injected intravitreally 1 hour prior to retinal insult. Both LXA_4 and LXB_4 treatments significantly ($P < 0.01$) increased RGC survival, by 57% (±3.8) and 99% (±4.7), respectively, compared with vehicle (Figure 4, A and B). Unexpectedly, LXB_4 was

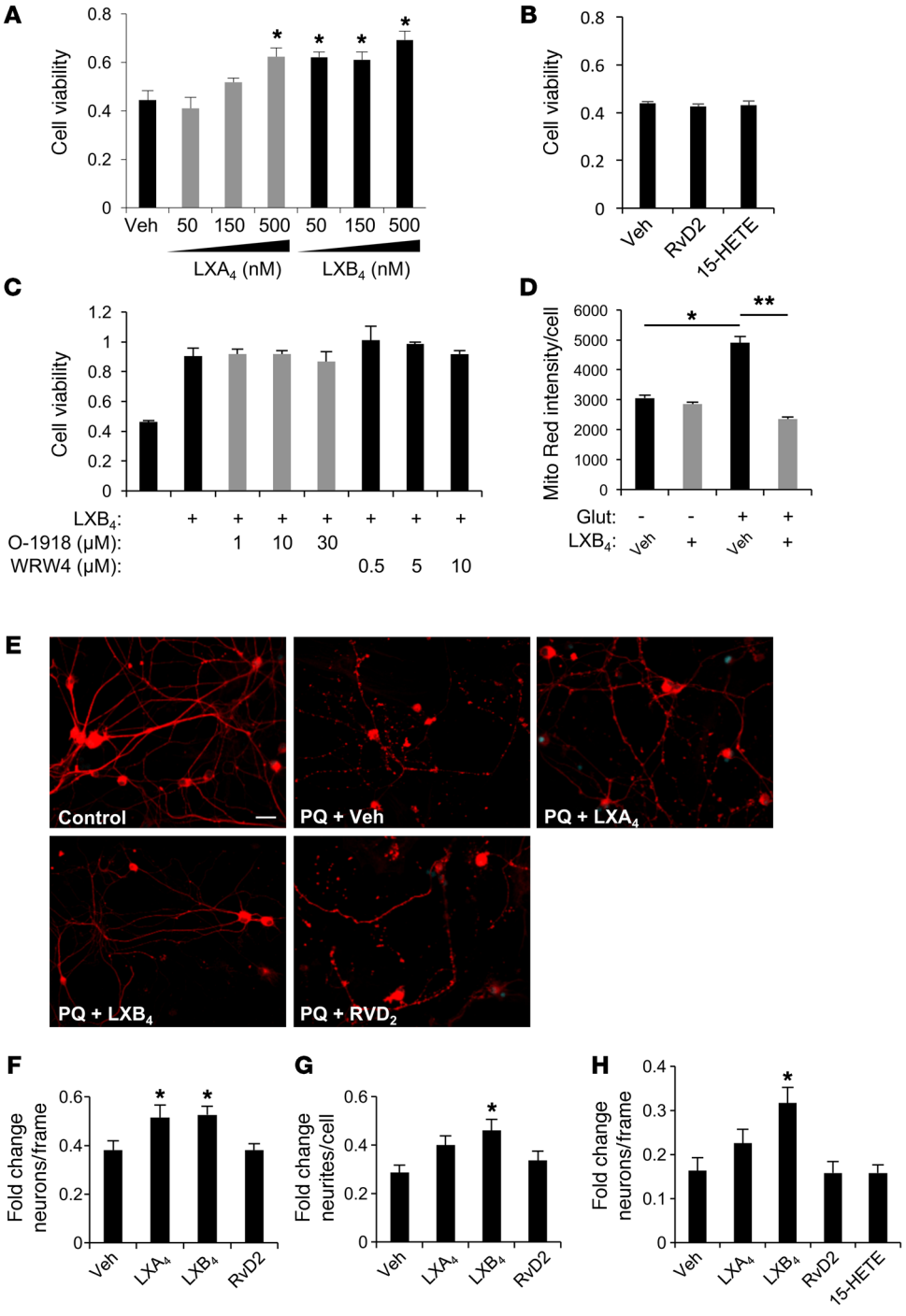

Figure 5. LXA_4 and LXB_4 have direct neuroprotective activities. (**A**) Treatment of HT22 neuronal cells with LXA_4 or LXB_4 significantly protected them from metabolic insult in a dose-dependent manner up to 500 nM (n = 3). (**B**) No protective activity was observed by treatment with up to 1 μM of the related molecules 15-HETE or RvD2 (n = 3). (**C**) LXB_4 protective activity at 500 nM was not blocked by treatment with increasing μM concentrations of WRW4 or the GPR18 antagonist O-1918 (n = 3). (**D**) MitoTracker red signal indicates protection from increased membrane potential with LXB_4 treatment (n = 3) (**E**) Primary RGCs labeled with β3-tubulin extend an extensive network of neurites that disintegrate dramatically after 24 hours of 30 μM PQ. Intact neurites are significantly maintained by 1 μM LXB_4, but not LXA_4 or RvD2. (**F**) RGC survival following oxidative stress demonstrates significant rescue with treatment by LXA_4 or LXB_4 (n = 3). (**G**) RGC neurite degeneration following PQ challenge was significantly rescued by LXB_4, but not LXA_4 or RvD2 (n = 3). (**H**) Primary cortical neurons demonstrate a similar protective effect for LXB_4 (n = 5). Scale bar: 20 μm. $^*P < 0.05$; $^{**}P < 0.01$. Bars represent SEM. Statistical analyses were performed by 1-way ANOVA with TUKEY post-hoc test.

more effective than LXA_4. As an alternative approach, we blocked lipoxin biosynthesis by administering a selective 5-LOX inhibitor, zileuton. Intravitreal zileuton alone had no effect on RGC numbers (Supplemental Figure 3), but significantly exacerbated RGC loss in response to injury, by 60% (±1.2) (Figure 4, C and D). We also administered a selective ALX/FPR2 inhibitor, WRW4, which also had no effect on RGC survival alone (Supplemental Figure 3), but increased RGC loss by 67% (±1.8) (Figure 4, E and F). Together, these data provide evidence that lipoxins are protective to RGCs in vivo and that their endogenous biosynthesis and signaling are necessary for acute retinal injury responses.

LXA_4 and LXB_4 provide direct neuroprotection. To determine whether the protective activity we observed was direct, we treated neuronal cells with LXA_4 or LXB_4 in our established in vitro assay. Increasing concentrations of LXA_4 or LXB_4 produced increased viability of glutamate-challenged HT22 cells (Figure 5A). Consistent with our in vivo results, LXB_4 appeared more potent than LXA_4, with significant activity at 50 nM versus 500 nM, respectively (Figure 5A). A subsequent dose-response curve generated an EC_{50} for LXB_4 of 39.2 nM and for LXA_4 of 631.0 nM, indicating a 16-fold increase in potency, though with similar efficacy (Supplemental Figure 4). In contrast, neither the lipoxin precursor 15-HETE nor

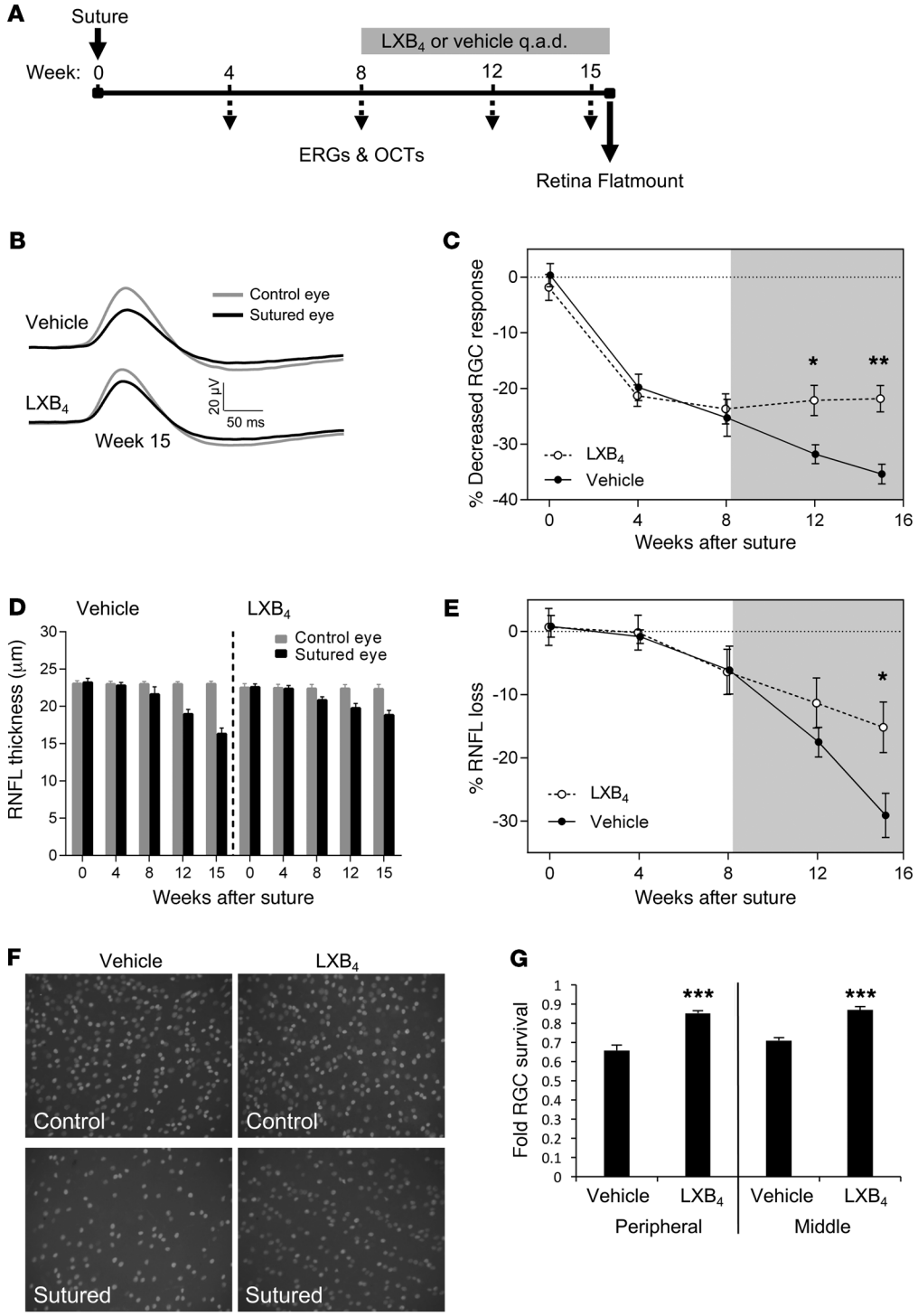

Figure 6. Therapeutic LXB_4 protects RGC function and survival following glaucomatous injury. (**A**) Experimental schematic showing ERG and OCT readings every 4 weeks following suture-induced IOP elevation. LXB_4 administration started at week 8, and retinal flatmounting and RGC counting were performed at week 15. q.a.d., every other day. (**B**) Average waveforms with an intensity of –4.60 log cd.s.m^{-2} for RGC (pSTR) responses at week 15 for LXB_4 and vehicle groups and (**C**) relative change in RGC function across 15 weeks. Starting at week 12, there was significant and increasing rescue of RGC response in LXB_4-treated eyes compared with vehicle (n = 8 per group). (**D**) RNFL thickness was monitored by OCT across 15 weeks, comparing sutured to control eyes in LXB_4- and vehicle-treated groups. (**E**) RNFL loss is significantly reduced in the LXB_4 group compared with vehicle at week 15 (n = 8). (**F**) Representative retinal flatmounts stained for BRN3a after 15 weeks of elevated IOP compared with contralateral control eyes from LXB_4- or vehicle-treated animals. Original magnification: ×20. (**G**) Quantification of RGC density shows significant rescue of RGC loss by LXB_4 treatment in central and peripheral retinas compared with vehicle (n = 8). *P < 0.05; **P < 0.01; ***P < 0.005. Bars represent SEM. Shaded area indicates the treatment period (**A**, **C**, and **E**). Statistical values were analyzed by 2-way ANOVA with Bonferroni post-hoc test (**C**–**E**) and by t test (**G**).

the structurally related trihydroxy SPM RvD2 had any protective activity up to 1 μM (Figure 5B). There is no established receptor for LXB_4. However, LXA_4 and RvD2 signal via the ALX/FPR2 and GPR18 receptors (31), respectively. Therefore, we assessed whether ALX/FPR2 or GPR18 antagonists could block LXB_4-mediated protection. Increasing concentrations of WRW4 (ALX/FPR2 antagonist; IC_{50} = 0.23 μM) or O-1918 (GPR18 antagonist; IC_{50} = 5.3 μM) did not block LXB_4-protective activity (Figure 5C). To further clarify the LXB_4 effect on cell viability, we also assessed mitochondrial membrane potential. LXB_4 treatment had no effect on membrane potential alone, but strongly protected against glutamate-induced activity compared with vehicle (Figure 5D and Supplemental Figure 5). These data suggest that LXB_4 neuroprotection is mediated through a distinct signaling mechanism influencing mitochondrial activity independently of LXA_4 or RvD2.

To confirm this activity in primary neurons, we tested the ability of LXA_4 or LXB_4 to protect RGCs. RGCs were isolated by immunopanning and challenged by PQ-induced oxidative stress. Cell

and neurite survival were then quantified in a series of β3-tubulin–stained images for each group. Under normal culture conditions, the RGCs extended an extensive network of neurites (Figure 5E). However, after 24 hours of PQ exposure, both neurite and cell numbers were reduced (Figure 5, E–G). Treatment with 1 μM of either LXA_4 or LXB_4 significantly rescued RGC numbers (Figure 5F). However, only LXB_4 significantly reduced neurite degeneration (Figure 5G). In comparison, RvD2 had no protective activity in either parameter (Figure 5, E–G). Similar protective LXB_4 activity was observed for primary cortical neurons (Figure 5H) or when RGCs were challenged with serum deprivation (SD) (Supplemental Figure 6). Therefore, LXB_4 demonstrates broad and distinct neuroprotective activity that is independent of established LXA_4 signaling.

Therapeutic LXB_4 treatment rescues RGC function and survival in a chronic glaucoma model. To assess whether lipoxin neuroprotective actions extend to chronic neurodegenerative injury, we investigated a rat circumlimbal suture model of glaucoma. In this assay, sustained intraocular pressure (IOP) elevation can be consistently maintained over 15 weeks (32, 33), resulting in compromised RGC function, reduced retinal nerve fiber layer (RNFL) thickness, and RGC death (32). As RGC functional deficits are reversible for up to 8 weeks (33), we chose this time point to initiate therapeutic treatment of LXB_4 or vehicle (Figure 6A). Electroretinogram (ERG) and optical coherence tomography (OCT) were measured monthly to assess retinal structure and function. We focused on LXB_4 for this challenging study due to its consistently higher potency than LXA_4 in our acute assays.

Importantly, IOP levels in the LXB_4 group did not differ from those in the vehicle group, eliminating a potential indirect effect (Supplemental Figure 7). However, by week 12, the positive scotopic threshold response (pSTR, an RGC-dependent ERG signal) showed significant preservation in RGC function in the LXB_4 group compared with vehicle. This protection continued to week 15, while the vehicle group continued to decline ($P < 0.05$) (Figure 6, B and C). Similarly, OCT measurement of RNFL thickness reflecting axonal loss was significantly rescued in the LXB_4-treatment group compared with the vehicle group by week 15 ($P < 0.05$) (Figure 6, D and E). These results were specific to inner retinal injury, as there was minimal effect on other ERG parameters and no decline in total retinal thickness (Supplemental Figure 8). To confirm these results, animals were euthanized at week 15 and flat-mounted retinas were stained for BRN3a. LXB_4-treated retinas presented a significant rescue of RGCs in both peripheral and central retinal regions compared with vehicle ($P < 0.005$) (Figure 6, F and G, and Supplemental Figure 9), although there was still cell loss in both groups. Together, these data demonstrate that therapeutic LXB_4 administration provides substantial protective effect in RGC function and survival in a model of chronic glaucoma.

Discussion

Neurodegeneration in response to stress or injury has been associated with both the induction of neuroinflammatory signals (34–37) and a corresponding loss of homeostatic prosurvival cues (38–41). However, the mechanisms by which these activities are coordinated in the CNS remain unclear. This study provides the first evidence, to our knowledge, that astrocyte-released LXA_4 and LXB_4 have direct protective neuronal actions that are compromised following neuronal injury in addition to their proresolving roles. Under normal conditions, astrocytes maintain a host of homeostatic support functions, but they transition to parainflammatory reactive states that can have both positive and negative non–cell autonomous influences on neighboring neurons (6, 42). In particular, Sun et al. have recently demonstrated beneficial effects of astrocyte remodeling in the ONH, but did not describe an underlying molecular mechanism (4). Our data suggest that, together, astrocyte-derived LXA_4 and LXB_4 help coordinate a protective signal in the retina and ONH, while simultaneously dampening neuroinflammation. This mechanism would complement a classification proposed by Zamanian et al., in which reactive astrocytes can transition from homeostatic quiescent to either neurotoxic A1 or protective A2 states (3, 5), although we cannot rule out potential autocrine contributions from neurons as well. Thus, regulation of lipoxin levels may help coordinate between paracrine neuroinflammatory and neuroprotective processes.

SPM dysregulation has been implicated in neuroinflammation related to Alzheimer's disease, stroke, and age-related macular degeneration (17, 18). Additionally, mice deficient in A*LOX5* or *ALOX15* have increased vulnerability in models of multiple sclerosis (MS) and Huntington's disease (43, 44). Yet most SPM actions have been linked to their established antiinflammatory and proresolving activities. To our knowledge, only the structurally distinct DHA derivative, NPD1, has been linked directly to neuroprotective actions (45, 46). The lipoxins were the first identified and remain the only AA-derived SPMs. AA is the most abundant substrate for lipoxygenase enzymes in most tissues, and LXA_4 has been detected throughout the CNS (24, 47) and in human vitreous (48). Additionally, endogenous and aspirin-triggered lipoxins have been shown to reduce inflammatory pain processing through effects on astrocytes (49). However, the generation of lipoxins by astrocytes and their direct neuroprotective actions have not been reported, and the present findings would likely not have been detected in a more conventional genomic or proteomic screen.

Surprisingly, LXB_4 was consistently more potent in our in vitro and in vivo experiments than LXA_4, with a significant rescue of neurite survival and altered mitochondrial activity. Yet the 2 molecules are structural isomers and are inactivated by the same enzymatic pathways (50). Our evidence demonstrates a complete lipoxin synthetic and signaling circuit in astrocytes and the inner retina, while ALX/FPR2 inhibition suggests that LXA_4 signaling plays a role in acute injury. In comparison, the formation and bioactions of LXB_4 have not been fully investigated, but it has been shown to block TNF-α secretion by activated T cells (51), and its production is regulated by NLRP3 inflammasome activity (52). We observed that inhibition of the LXA_4 receptor (ALX/FPR2) or RvD2 receptor (GPR18) was insufficient to block protective LXB_4 activity. Likewise, neither 15-HETE nor RvD2 showed any direct neuroprotection, suggesting that LXB_4 signaling is specific and distinct from LXA_4 and the structurally related DHA series resolvin RvD2 (31). Hence, LXB_4 signaling warrants further investigation with respect to its neuroprotective role.

Glaucoma is a common neurodegenerative disease and a leading cause of vision loss and blindness worldwide, projected to afflict 76 million people by 2020 (53, 54). Elevated IOP is the most established, and only treatable, glaucoma risk factor. However,

many patients do not exhibit elevated IOP, and nearly all patients eventually progress (8, 53, 55). In this respect, glaucoma shares the complex etiology common to related neurodegenerative processes throughout the CNS (7, 8, 10) and may involve both non–cell-autonomous and cell-autonomous RGC death mechanisms (10, 56). Yet no neuroprotective treatment is available, representing a major health challenge (57). In our experiments, therapeutic LXB_4 treatment was efficacious in clinically relevant measures of ERG (RGC function) and OCT (axonal loss) and in reducing RGC death. However, LXB_4 had no effect on IOP. Taken together, our results strikingly suggest LXB_4 mediates neuroprotection of RGC function and survival in a therapeutic context under conditions of chronic IOP-induced injury. These promising findings support further research into the role and mechanisms of lipoxin signaling during neuronal injury and exploration of their therapeutic potential in the context of neurodegeneration.

Methods

Mouse acute retinal insult model. Male C57BL/6 mice were anesthetized by i.p. injection of ketamine/xylazine. Intravitreal injections with 10 mM KA were performed as previously described (58). Similar excitotoxic damage models have been extensively used by ourselves and others to study the influence of retinal glia on neuronal survival and function, providing a consistent and accurate assessment of retinal neuropathology (12, 14, 30, 58–60). Briefly, a 30-gauge needle was inserted tangentially into the vitreous and replaced with a Hamilton syringe to inject a volume of 2 μl, followed by application of ophthalmic antibiotic ointment (BNP, Vetoquinol). In some experiments, 100,000 RAs were first injected 16 days prior to KA challenge. Alternatively 10× concentrated ACM or test compounds were injected intravitreally 24 hours or 1 hour, respectively, prior to the KA injection in the following concentrations: 10 μM LXA_4 and LXB_4, 2 μg/μl zileuton (a selective 5-LOX inhibitor that has been used clinically; refs. 61, 62), and 15 μM WRW4 (a selective ALX/FPR2 inhibitor; refs. 62–64), all dissolved in PBS. Mice were euthanized by CO_2 asphyxiation 18 hours after KA treatment, and the eyes were fixed in 4% paraformaldehyde. For RNA and lipidomics analyses, retinas and ONs were dissected and snap-frozen on dry ice. In all experiments, *n* refers to the number of animals tested.

Astrocyte cultures. Primary RAs were isolated and cultured as previously described (14, 27–29, 58). These cells display typical astrocyte morphology and a variety of appropriate markers, including GFAP, vimentin, Pax-2, GS, and S100A. They also respond robustly to oxidative and metabolic stress with changes in activation markers, secreted cytokines, and antioxidants (27, 58) (Supplemental Figure 1). Briefly, eyes were dissected out of adult Wistar rats and placed in ice-cold MEM-H17 with 10% FBS/1% penicillin/streptomycin. Isolated retinas were digested by shaking in MEM-H17 containing papain and DNAse, followed by trituration to disperse cell aggregates. When cultures reached confluence, the cells were placed on a rotating shaker for 6 to 8 hours to remove microglia and then replated. An astrocyte-expression profile was confirmed by probing the cultures with a panel of glial and neuronal markers (27). Note that efforts to generate a serum-free defined media resulted in cellular stress that compromised the protective activity. Therefore, conditioned media experiments contained serum, although control media exhibited no activity. RA conditioned medium (ACM) or cell-free control medium was harvested after 24 hours incubation and stored at –80°C.

Neuronal cultures. HT22 neuronal cells (65, 66) were cultured in high-glucose DMEM with 10% FBS/1% penicillin/streptomycin. For neuroprotection experiments, injury was induced by incubation with 5 mM glutamate. Cell viability was assessed by XTT assay and absorbance was measured at 490 nm, according to the manufacturer's directions (Roche). MitoTracker Red (Life Technologies) was used according to the manufacturer's instructions, with intensity per cell calculated for 42 cells for each well. RGCs were purified using magnetic MicroBeads (Miltenyi Biotec) according to the manufacturer's protocol. Briefly, retinal cell suspensions were prepared from 8- to 10-day-old rats and incubated with CD90.1 microbeads and biotinylated depletion antibodies against microglia and endothelial cells. Cells were gently centrifuged and washed with DPBS/BSA buffer. Resuspended cells were incubated with magnetic Anti-Biotin MACSi-Beads (Miltenyi Biotec) and applied to a MACs separation magnet. The preenriched population was applied to a MACs MS separation column twice to enrich for CD90.1-bound RGCs. RGCs were plated in poly-D-lysine–coated wells and cultured in Neurobasal-A media (GIBCO; Thermo Fisher Scientific) supplemented with 2% calf serum, 2% B27 supplement, 1 mM L-glutamine, 50 ng/ml BDNF, 50 ng/ml CNTF, 5 μM forskolin, and 1% penicillin/streptomycin. To assess RGC survival, cultures were challenged with serum and supplement deprivation or 30 μM PQ, fixed, probed for β3-tubulin, and imaged with a Nikon confocal microscope. The number of cell bodies and ratio of neurites/cell was established for each acquired frame, with 32 frames scored from each experimental group. Primary cortical neurons were cultured essentially as described (67). Briefly, cortices were dissected from E16 mouse embryos on ice. The tissue was homogenized and dissociated with papain and DNAse, triturated, and strained to remove clumps. Cortical neurons were seeded onto poly-D-lysine–coated wells with Neurobasal-A media with L-glutamine and B27 supplement. All data represent at least 3 independent experiments for each treatment.

LC-MS/MS. Eicosanoids and PUFA in the conditioned media were quantified via LC-MS/MS according to our published protocol (61, 68–70). Briefly, class-specific deuterated internal standards (PGE_2-d4, LTB4-d4, 15-HETE-d8, LXA_4-d5, DHA-d5, AA-d8) were used to calculate extraction recovery on an LC-MS/MS system consisting of an Agilent 1200 Series HPLC, Kinetex C18 minibore column (Phenomenex), and AB Sciex QTRAP 4500 system. Analysis was carried out in negative ion mode, and eicosanoids and PUFA were quantitated using scheduled multiple reaction monitoring (MRM) using from 4 to 6 specific transition ions for each analyte. We used specific retention time and established prominent fragment ions for identification and quantification of LXB_4 and LXA_4 (52, 71, 72). Prominent fragment ions for identification of LXB_4 (351.2 m/z, retention time 8.9 minutes) included 115.1, 189.2, 221.1, 217.3, 251.1, and for LXA_4 (351.2 m/z, retention time 10.5 minutes) fragment ions included 115.1, 135.1, 189.2, 217.3, and 235.3. Calibration curves were established with synthetic standards (Cayman Chemicals).

qPCR. Mouse retinal mRNA was isolated using RNeasy Isolation Kit (QIAGEN), quantified using NanoDrop, and mRNA reverse transcribed with the High Capacity cDNA Kit (Applied Biosystems). qPCR was performed with SYBR Green Master Mix (Applied Biosystems) using the ΔΔCt method in the StepOnePlus qPCR System (Applied Biosystems). β-Actin was used as the reference gene. The primers used were as follows: β-actin: forward, ACGGCCAGGTCATCACTATTG, reverse, AGGGGCCGGACTCATCGTA; 5-LOX: forward,

ACTACATCTACCTCAGCCTCATT, reverse, GGTGACATCGTAGGAGTCCAC; 12/15-LOX: forward, GCGACGCTGCCCAATCCTAATC, reverse, ATATGGCCACGCTGTTTTCTACC; FPR2 (ALX): forward, GCCAGGACTTTCGTGGAGAGAT, reverse, GATGAACTGGTGCTTGAATCACT.

Immunofluorescence microscopy. Following fixation, eyes were equilibrated in 30% sucrose, embedded in optimal cutting temperature compound, and cryosectioned. Sections were blocked and probed with primary antibodies to GFAP (Sigma-Aldrich), CD68, GR-1 and F4/80 (BioLegend), FPR2 (Abnova), RBPMS (PhosphoSolutions), BRN3a (Santa Cruz Biotechnology Inc.), and 5-LOX (Millipore) according to standard protocols. Following PBS-Tween washes, sections were incubated with fluorescent-conjugated secondary antibodies (Molecular Probes) and mounted with medium containing DAPI. TUNEL staining was performed according to the manufacturer's instructions (DeadEnd; Promega). Briefly, sections were fixed with 4% PFA for 5 minutes and washed in PBS. Equilibrium buffer was added, and rTdT reaction mix was applied to each slide at 37°C for 60 minutes. Slides were immersed in 2× SSC and then washed with PBS. This was followed by blocking with 5% goat serum and overnight incubation with primary antibodies at 4°C. Immunofluorescent images were acquired with a Zeiss Axio Imager microscope and a Nikon Eclipse-Ti confocal microscope.

Quantification of RGC survival. For in vivo experiments, RBPMS-positive cells in the GCL were counted and expressed as a fraction of total GCL nuclei. For each eye, at least 5 central retinal sections were analyzed at the level of the ON to the periphery and the results averaged, as previously described (14). In parallel, TUNEL-positive GCL nuclei were counted and expressed as a fraction of the total GCL nuclei (58, 73–76). For in vitro experiments, RGCs were isolated, treated, and probed with an antibody to β3-tubulin and imaged as above. A total of 32 frames from each experimental group were scored for the number of cell bodies and intact neurites. The ratio of neurites to RGC cell bodies was established for each acquired frame.

Rat chronic IOP-elevation model. A method for reliably inducing sustained IOP elevation in the rodent eye was recently developed by Liu et al. (32, 77). In this minimally invasive approach, a circumlimbal suture is placed to induce mild chronic ocular hypertension for up to 15 weeks (32). Elevated IOP is the primary clinical glaucoma risk factor, and this model results in similar compromised RGC function, reduced RNFL thickness, and death of RGCs by week 15 (32). Therefore, this model provides an opportunity to assess therapeutic neuroprotective activity in a chronic degenerative environment. Elevated IOP and RGC functional deficits are reversible with suture removal for up to 8 weeks (33). We therefore chose week 8 after IOP elevation to initiate therapeutic treatment of either vehicle or LXB_4 along with longitudinal and pathological assessment of RGC function and survival. Circumlimbal sutures were placed monocularly in the randomized eyes of anesthetized rats using a sterile 8-0 nylon suture. IOP was measured twice a week, and only animals showing sustained elevated IOP over 21 mmHg for the duration of the experiment were included in the analyses. The delivery and dosage of LXB_4 were based on previous publications (78–80). Briefly, LXB_4 or PBS vehicle was administered 3 times a week starting from week 8. Due to a short half-life and to ensure consistent retinal delivery, the lipoxin treatment protocol consisted of i.p. injection (1 μg) and topical application to each eye (100 ng). ERG was measured monthly to assess RGC functional changes using the pSTR, as we previously used it to measure the impact of elevated chronic IOP (32, 81). In addition, RNFL and total retinal thickness were quantified once a month using OCT. After 15 weeks, animals were euthanized and RGC numbers were counted on central (2000 μm from ON head) and peripheral (4000 μm from ON head) regions of retinal flatmounts following immunofluorescent staining for BRN3a as above.

Statistics. For all experiments, *n* refers to the number of animals or biological replicates. Dose-response data for LXA_4 and LXB_4 were fitted to logistic curves, using SigmaPlot 11.0 (Systat Software Inc.) and used to determine Emax (efficacy) and EC_{50} values. For TUNEL staining and RGC counts, statistical analyses were performed by *t* test or 1-way ANOVA with Tukey's post hoc analyses. ERG and OCT results were analyzed by 2-way ANOVA with Bonferroni's post hoc test.

Study approval. All experimental protocols were approved by the University Health Network and University of California at Berkeley's ACUCs in accordance with applicable regulations.

Author contributions

ILB conceived, performed, and analyzed in vitro and in vivo experiments, prepared figures, and helped write the manuscript. JW conceived and performed lipidomic analyses and PCR and prepared figures. HHL performed and analyzed the chronic IOP model and prepared figures. SA, AT, and GJW conceived and performed in vitro experiments. KG and JGF conceived experiments, analyzed data, and helped with manuscript editing. JMS conceived experiments, analyzed data, prepared figures, and wrote the manuscript. All authors reviewed the results and approved the final version of the manuscript.

Acknowledgments

The authors thank Rod Bremner, Jeff Wrana, Xiaoxin Guo, Darren Chan, Marinie Joseph, Victoria Ly, Adrian Nahirnyj, and Susy Lam. Support was provided by the Canadian Institutes of Health Research (CIHR) (MOP123448 to JMS and JGF), the NIH (EY026082 to KG), the Natural Sciences and Engineering Research Council of Canada (NSERC 06561 to JMS), the Glaucoma Research Society of Canada (GRSC) (to JMS), and a Glaucoma Research Foundation Shaffer Grant (to JGF). JMS is the Toronto General and Western Hospital Foundation Glaucoma Research Chair.

Address correspondence to: Jeremy M. Sivak, Department of Vision Sciences, Krembil Research Institute, 60 Leonard Avenue, Toronto, Ontario, Canada M5T 2S8. Phone: 416.507.6845; Email: jsivak@uhnres.utoronto.ca.

1. Liddelow S, Barres B. SnapShot: astrocytes in health and disease. *Cell*. 2015;162(5):1170–1170.e1.
2. Parpura V, et al. Glial cells in (patho)physiology. *J Neurochem*. 2012;121(1):4–27.
3. Liddelow SA, et al. Neurotoxic reactive astrocytes are induced by activated microglia. *Nature*. 2017;541(7638):481–487.
4. Sun D, Moore S, Jakobs TC. Optic nerve astrocyte reactivity protects function in experimental glaucoma and other nerve injuries. *J Exp Med*. 2017;214(5):1411–1430.
5. Zamanian JL, et al. Genomic analysis of reactive astrogliosis. *J Neurosci*. 2012;32(18):6391–6410.
6. Pekny M, Pekna M. Astrocyte reactivity and reactive astrogliosis: costs and benefits. *Physiol Rev*. 2014;94(4):1077–1098.
7. Sivak JM. The aging eye: common degenerative mechanisms between the Alzheimer's brain

and retinal disease. *Invest Ophthalmol Vis Sci*. 2013;54(1):871–880.
8. Weinreb RN, et al. Primary open-angle glaucoma. *Nat Rev Dis Primers*. 2016;2:16067.
9. Hernandez MR, Miao H, Lukas T. Astrocytes in glaucomatous optic neuropathy. *Prog Brain Res*. 2008;173:353–373.
10. Almasieh M, Wilson AM, Morquette B, Cueva Vargas JL, Di Polo A. The molecular basis of retinal ganglion cell death in glaucoma. *Prog Retin Eye Res*. 2012;31(2):152–181.
11. Tezel G, Wax MB. Increased production of tumor necrosis factor-alpha by glial cells exposed to simulated ischemia or elevated hydrostatic pressure induces apoptosis in cocultured retinal ganglion cells. *J Neurosci*. 2000;20(23):8693–8700.
12. Lebrun-Julien F, et al. ProNGF induces TNF-alpha-dependent death of retinal ganglion cells through a p75NTR non-cell-autonomous signaling pathway. *Proc Natl Acad Sci U S A*. 2010;107(8):3817–3822.
13. Yuan L, Neufeld AH. Tumor necrosis factor-alpha: a potentially neurodestructive cytokine produced by glia in the human glaucomatous optic nerve head. *Glia*. 2000;32(1):42–50.
14. Livne-Bar I, et al. Pharmacologic inhibition of reactive gliosis blocks TNF-α-mediated neuronal apoptosis. *Cell Death Dis*. 2016;7(9):e2386.
15. Gronert K. Lipid autacoids in inflammation and injury responses: a matter of privilege. *Mol Interv*. 2008;8(1):28–35.
16. Serhan CN. Pro-resolving lipid mediators are leads for resolution physiology. *Nature*. 2014;510(7503):92–101.
17. Gordon WC, Bazan NG. Mediator lipidomics in ophthalmology: targets for modulation in inflammation, neuroprotection and nerve regeneration. *Curr Eye Res*. 2013;38(10):995–1005.
18. Serhan CN, Dalli J, Colas RA, Winkler JW, Chiang N. Protectins and maresins: New pro-resolving families of mediators in acute inflammation and resolution bioactive metabolome. *Biochim Biophys Acta*. 2015;1851(4):397–413.
19. Ryan A, Godson C. Lipoxins: regulators of resolution. *Curr Opin Pharmacol*. 2010;10(2):166–172.
20. Serhan CN, Hamberg M, Samuelsson B. Lipoxins: novel series of biologically active compounds formed from arachidonic acid in human leukocytes. *Proc Natl Acad Sci U S A*. 1984;81(17):5335–5339.
21. Maddox JF, Hachicha M, Takano T, Petasis NA, Fokin VV, Serhan CN. Lipoxin A4 stable analogs are potent mimetics that stimulate human monocytes and THP-1 cells via a G-protein-linked lipoxin A4 receptor. *J Biol Chem*. 1997;272(11):6972–6978.
22. Czapski GA, Czubowicz K, Strosznajder JB, Strosznajder RP. The lipoxygenases: their regulation and implication in Alzheimer's disease. *Neurochem Res*. 2016;41(1-2):243–257.
23. Martini AC, Forner S, Bento AF, Rae GA. Neuroprotective effects of lipoxin A4 in central nervous system pathologies. *Biomed Res Int*. 2014;2014:316204.
24. Wang X, et al. Resolution of inflammation is altered in Alzheimer's disease. *Alzheimers Dement*. 2015;11(1):40–50.e1.
25. Romano M, Maddox JF, Serhan CN. Activation of human monocytes and the acute monocytic leukemia cell line (THP-1) by lipoxins involves unique signaling pathways for lipoxin A4 versus lipoxin B4: evidence for differential Ca2+ mobilization. *J Immunol*. 1996;157(5):2149–2154.
26. Fiore S, Maddox JF, Perez HD, Serhan CN. Identification of a human cDNA encoding a functional high affinity lipoxin A4 receptor. *J Exp Med*. 1994;180(1):253–260.
27. Nahirnyj A, Livne-Bar I, Guo X, Sivak JM. ROS detoxification and proinflammatory cytokines are linked by p38 MAPK signaling in a model of mature astrocyte activation. *PLoS ONE*. 2013;8(12):e83049.
28. Rogers RS, Dharsee M, Ackloo S, Sivak JM, Flanagan JG. Proteomics analyses of human optic nerve head astrocytes following biomechanical strain. *Mol Cell Proteomics*. 2012;11(2):M111.012302.
29. Exler RE, et al. Biomechanical insult switches PEA-15 activity to uncouple its anti-apoptotic function and promote erk mediated tissue remodeling. *Exp Cell Res*. 2016;340(2):283–294.
30. Ganesh BS, Chintala SK. Inhibition of reactive gliosis attenuates excitotoxicity-mediated death of retinal ganglion cells. *PLoS ONE*. 2011;6(3):e18305.
31. Chiang N, Dalli J, Colas RA, Serhan CN. Identification of resolvin D2 receptor mediating resolution of infections and organ protection. *J Exp Med*. 2015;212(8):1203–1217.
32. Liu HH, Bui BV, Nguyen CT, Kezic JM, Vingrys AJ, He Z. Chronic ocular hypertension induced by circumlimbal suture in rats. *Invest Ophthalmol Vis Sci*. 2015;56(5):2811–2820.
33. Liu HH, He Z, Nguyen CT, Vingrys AJ, Bui BV. Reversal of functional loss in a rat model of chronic intraocular pressure elevation. *Ophthalmic Physiol Opt*. 2017;37(1):71–81.
34. Chung WS, Welsh CA, Barres BA, Stevens B. Do glia drive synaptic and cognitive impairment in disease? *Nat Neurosci*. 2015;18(11):1539–1545.
35. Doty KR, Guillot-Sestier MV, Town T. The role of the immune system in neurodegenerative disorders: Adaptive or maladaptive? *Brain Res*. 2015;1617:155–173.
36. Klein RS, Garber C, Howard N. Infectious immunity in the central nervous system and brain function. *Nat Immunol*. 2017;18(2):132–141.
37. Xu H, Chen M, Forrester JV. Para-inflammation in the aging retina. *Prog Retin Eye Res*. 2009;28(5):348–368.
38. Mariga A, Mitre M, Chao MV. Consequences of brain-derived neurotrophic factor withdrawal in CNS neurons and implications in disease. *Neurobiol Dis*. 2017;97(Pt B):73–79.
39. Levi-Montalcini R, Booker B. Destruction of the sympathetic ganglia in mammals by an antiserum to a nerve-growth protein. *Proc Natl Acad Sci U S A*. 1960;46(3):384–391.
40. Cohen-Cory S, Fraser SE. Effects of brain-derived neurotrophic factor on optic axon branching and remodelling in vivo. *Nature*. 1995;378(6553):192–196.
41. Hofer MM, Barde YA. Brain-derived neurotrophic factor prevents neuronal death in vivo. *Nature*. 1988;331(6153):261–262.
42. Zuchero JB, Barres BA. Glia in mammalian development and disease. *Development*. 2015;142(22):3805–3809.
43. Emerson MR, LeVine SM. Experimental allergic encephalomyelitis is exacerbated in mice deficient for 12/15-lipoxygenase or 5-lipoxygenase. *Brain Res*. 2004;1021(1):140–145.
44. He Y, Akumuo RC, Yang Y, Hewett SJ. Mice deficient in L-12/15 lipoxygenase show increased vulnerability to 3-nitropropionic acid neurotoxicity. *Neurosci Lett*. 2017;643:65–69.
45. Bazan NG. Neuroprotectin D1 (NPD1): a DHA-derived mediator that protects brain and retina against cell injury-induced oxidative stress. *Brain Pathol*. 2005;15(2):159–166.
46. Calandria JM, et al. NPD1-mediated stereoselective regulation of BIRC3 expression through cREL is decisive for neural cell survival. *Cell Death Differ*. 2015;22(8):1363–1377.
47. Martini AC, et al. Lipoxin A4 inhibits microglial activation and reduces neuroinflammation and neuropathic pain after spinal cord hemisection. *J Neuroinflammation*. 2016;13(1):75.
48. Kaviarasan K, et al. Low blood and vitreal BDNF, LXA4 and altered Th1/Th2 cytokine balance are potential risk factors for diabetic retinopathy. *Metab Clin Exp*. 2015;64(9):958–966.
49. Svensson CI, Zattoni M, Serhan CN. Lipoxins and aspirin-triggered lipoxin inhibit inflammatory pain processing. *J Exp Med*. 2007;204(2):245–252.
50. Maddox JF, Serhan CN. Lipoxin A4 and B4 are potent stimuli for human monocyte migration and adhesion: selective inactivation by dehydrogenation and reduction. *J Exp Med*. 1996;183(1):137–146.
51. Ariel A, Chiang N, Arita M, Petasis NA, Serhan CN. Aspirin-triggered lipoxin A4 and B4 analogs block extracellular signal-regulated kinase-dependent TNF-alpha secretion from human T cells. *J Immunol*. 2003;170(12):6266–6272.
52. Lee S, et al. NLRP3 Inflammasome Deficiency Protects against Microbial Sepsis via Increased Lipoxin B4 Synthesis. *Am J Respir Crit Care Med*. 2017;196(6):713–726.
53. Tham YC, Li X, Wong TY, Quigley HA, Aung T, Cheng CY. Global prevalence of glaucoma and projections of glaucoma burden through 2040: a systematic review and meta-analysis. *Ophthalmology*. 2014;121(11):2081–2090.
54. Kwon YH, Fingert JH, Kuehn MH, Alward WL. Primary open-angle glaucoma. *N Engl J Med*. 2009;360(11):1113–1124.
55. Heijl A, et al. Reduction of intraocular pressure and glaucoma progression: results from the Early Manifest Glaucoma Trial. *Arch Ophthalmol*. 2002;120(10):1268–1279.
56. Maes ME, Schlamp CL, Nickells RW. BAX to basics: How the BCL2 gene family controls the death of retinal ganglion cells. *Prog Retin Eye Res*. 2017;57:1–25.
57. Calkins DJ, Pekny M, Cooper ML, Benowitz L, Lasker/IRRF Initiative on Astrocytes Glaucomatous Neurodegeneration Participants. The challenge of regenerative therapies for the optic nerve in glaucoma. *Exp Eye Res*. 2017;157:28–33.
58. Guo X, et al. PGC-1α signaling coordinates susceptibility to metabolic and oxidative injury in the inner retina. *Am J Pathol*. 2014;184(4):1017–1029.
59. Gomez-Ramos P, Reinoso-Suarez F. Kainic acid prevents peroxidase labeling of retinal ganglion cell bodies in the rat: a possible gate in retrograde

axonal transport. *Neurosci Lett*. 1983;35(1):1–6.
60. Wang Q, Yu S, Simonyi A, Sun GY, Sun AY. Kainic acid-mediated excitotoxicity as a model for neurodegeneration. *Mol Neurobiol*. 2005;31(1-3):3–16.
61. Sapieha P, et al. 5-Lipoxygenase metabolite 4-HDHA is a mediator of the antiangiogenic effect of ω-3 polyunsaturated fatty acids. *Sci Transl Med*. 2011;3(69):69ra12.
62. Smith HK, Gil CD, Oliani SM, Gavins FN. Targeting formyl peptide receptor 2 reduces leukocyte-endothelial interactions in a murine model of stroke. *FASEB J*. 2015;29(5):2161–2171.
63. Fang X, et al. Human mesenchymal stem (stromal) cells promote the resolution of acute lung injury in part through lipoxin A4. *J Immunol*. 2015;195(3):875–881.
64. He N, Jin WL, Lok KH, Wang Y, Yin M, Wang ZJ. Amyloid-β(1-42) oligomer accelerates senescence in adult hippocampal neural stem/progenitor cells via formylpeptide receptor 2. *Cell Death Dis*. 2013;4:e924.
65. Lee Y, et al. Proteomic analysis of glutamate-induced toxicity in HT22 cells. *Proteomics*. 2007;7(2):185–193.
66. Stanciu M, et al. Persistent activation of ERK contributes to glutamate-induced oxidative toxicity in a neuronal cell line and primary cortical neuron cultures. *J Biol Chem*. 2000;275(16):12200–12206.
67. Sidorova-Darmos E, et al. Differential expression of sirtuin family members in the developing, adult, and aged rat brain. *Front Aging Neurosci*. 2014;6:333.
68. Hassan IR, Gronert K. Acute changes in dietary omega-3 and omega-6 polyunsaturated fatty acids have a pronounced impact on survival following ischemic renal injury and formation of renoprotective docosahexaenoic acid-derived protectin D1. *J Immunol*. 2009;182(5):3223–3232.
69. Murphy RC, et al. Electrospray ionization and tandem mass spectrometry of eicosanoids. *Anal Biochem*. 2005;346(1):1–42.
70. Serhan CN, Lu Y, Hong S, Yang R. Mediator lipidomics: search algorithms for eicosanoids, resolvins, and protectins. *Meth Enzymol*. 2007;432:275–317.
71. Colas RA, Shinohara M, Dalli J, Chiang N, Serhan CN. Identification and signature profiles for pro-resolving and inflammatory lipid mediators in human tissue. *Am J Physiol Cell Physiol*. 2014;307(1):C39–C54.
72. Norris PC, Libreros S, Chiang N, Serhan CN. A cluster of immunoresolvents links coagulation to innate host defense in human blood. *Sci Signal*. 2017;10(490):eaan1471.
73. Chen L, et al. Role of the immune modulator programmed cell death-1 during development and apoptosis of mouse retinal ganglion cells. *Invest Ophthalmol Vis Sci*. 2009;50(10):4941–4948.
74. Harada C, et al. ASK1 deficiency attenuates neural cell death in GLAST-deficient mice, a model of normal tension glaucoma. *Cell Death Differ*. 2010;17(11):1751–1759.
75. Nishijima K, et al. Vascular endothelial growth factor-A is a survival factor for retinal neurons and a critical neuroprotectant during the adaptive response to ischemic injury. *Am J Pathol*. 2007;171(1):53–67.
76. Riesenberg AN, Liu Z, Kopan R, Brown NL. Rbpj cell autonomous regulation of retinal ganglion cell and cone photoreceptor fates in the mouse retina. *J Neurosci*. 2009;29(41):12865–12877.
77. Liu HH, Flanagan JG. A mouse model of chronic ocular hypertension induced by circumlimbal suture. *Invest Ophthalmol Vis Sci*. 2017;58(1):353–361.
78. Biteman B, et al. Interdependence of lipoxin A4 and heme-oxygenase in counter-regulating inflammation during corneal wound healing. *FASEB J*. 2007;21(9):2257–2266.
79. Börgeson E, et al. Lipoxin A4 attenuates obesity-induced adipose inflammation and associated liver and kidney disease. *Cell Metab*. 2015;22(1):125–137.
80. Dunn HC, et al. Restoration of lipoxin A4 signaling reduces Alzheimer's disease-like pathology in the 3xTg-AD mouse model. *J Alzheimers Dis*. 2015;43(3):893–903.
81. Fortune B, et al. Selective ganglion cell functional loss in rats with experimental glaucoma. *Invest Ophthalmol Vis Sci*. 2004;45(6):1854–1862.